

Interplay of orientational order and roughness in simulated thin film growth of anisotropically interacting particles

E. Empting,* N. Bader, and M. Oettel
*Institut für Angewandte Physik, Universität Tübingen,
 Auf der Morgenstelle 10, 72076 Tübingen, Germany*

Roughness and orientational order in thin films of anisotropic particles are investigated using kinetic Monte Carlo simulations on a cubic lattice. Anisotropic next-neighbor interactions between the lattice particles were chosen to mimic the effects of shape anisotropy in the interactions of disc- or rod-like molecules with van-der-Waals attractions. Increasing anisotropy leads first to a preferred orientation in the film (which is close to the corresponding equilibrium transition) while the qualitative mode of roughness evolution (known from isotropic systems) does not change. At strong anisotropies, an effective step-edge (Ehrlich-Schwöbel) barrier appears and a non-equilibrium roughening effect is found, accompanied by re-ordering in the film which can be interpreted as the nucleation and growth of domains of lying-down discs or rods. The information on order and roughness is combined into a diagram of dynamic growth modes.

I. INTRODUCTION

Film growth of organic molecules is a topic of considerable practical interest, since it is an indispensable tool in the fabrication of organic optoelectronic devices¹. The morphology of such films, notably manifested in the film roughness or the orientation of molecules in the film, significantly influences the electronic properties of the resulting device². Besides the practical interest, film growth constitutes a basic non-equilibrium process for thermal many-body systems and is therefore of great theoretical relevance for the field of non-equilibrium statistical physics. Here, a large body of work has gone into the study of film growth with isotropic particles as realized in the growth of metal films. Roughness evolution is determined by the control parameters temperature, deposition speed and choice of substrate material³, and much insight and general results have been obtained using solid-on-solid (SOS) simulation models of particle growth on predefined lattices (very often taken to be a simple cubic lattice)^{4–15}. In recent work by our group, the transitions between different, basic modes of roughness evolution (layer-by-layer growth, island growth, rough growth from the start) which occur upon changing control parameters or happen as a function of the amount of deposited material, were studied¹⁶.

The workhorse SOS model on cubic lattices can be extended in several ways: One can investigate a system of multiple particle species¹⁷, different lattice types³, or introduce anisotropic particles. Anisotropy may be split into shape and interaction anisotropy. Here we mean by shape anisotropy that the steric core of particles is different from a sphere (continuum) or different from a cube (for models on cubic lattices). In contrast, interaction anisotropy refers to particles having an isotropic excluded volume interaction, but residual (attractive) interactions depend on the orientation of the particles. An example would be e.g. spherical particles with electric or magnetic multipole moments. The study of particles with anisotropic steric shapes

has a long history in investigations of the behavior of liquid crystals^{18,19}, while interaction anisotropy has been used to both study simple models of liquid crystals^{20,21} and the assembly of magnetic nano-cubes²² and to mimic effects of anisotropic substrates on film growth²³. Growth with organic molecules in general means that both shape and interaction anisotropy are involved. An exception is the growth of films with C_{60} ^{24,25}.

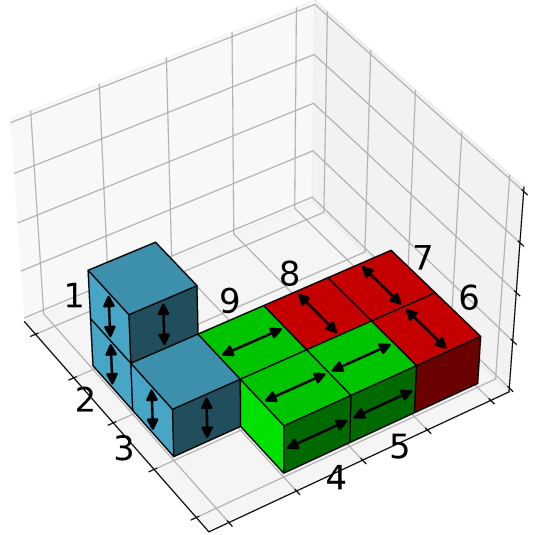


FIG. 1: Schematic representation of nearest-neighbor interactions. Colors and double arrows indicate particle orientations. Particle pairs 1-2, 4-5, and 6-7 each interact with strength $-\eta \cdot \epsilon$, since the particles in each pair are aligned along their respective orientational axes. All other particle pairs interact with strength $-\epsilon$. Additionally, particle in the lowest layer interact with the substrate with a strength $-\epsilon_{\text{sub}}$. Interactions are in units of the thermal energy $k_B T$.

In this work, we study by simulations the film growth with cubic particles possessing interaction anisotropy on cubic lattices. Particles are characterized by an orientation in ei-

* eelco.empting@uni-tuebingen.de

ther the x , y , or z direction, and if two particles of the same orientation are aligned in this orientation direction, their interaction is stronger by a factor of η . This particular form of anisotropy was chosen to mimic the shape of disc-like organic molecules, e.g. benzene or perylene (see the discussion in Sec. II B below). The fact that particles still only occupy one lattice site allows us to implement the solid-on-solid restriction, which prevents cavities inside the film and significantly reduces computational overhead. Despite the simplicity of the model, it depends on a number of parameters (particle-particle interaction, interaction anisotropy, substrate-particle interaction, lateral and rotational diffusion, growth rate) and we attempt a systematic study of the dependence on those parameters. The main focus is on the influence of the interaction anisotropy and orientational order in the film on the simple growth modes identified in Ref. 16 in the isotropic case. Previous work regarding lattice film growth has usually focused on either the sub-monolayer regime or on long-time scaling behavior. In contrast to this, we are interested in the evolution of roughness and orientation during the growth of a “medium-thick” film. We find that for small interaction anisotropies, there is a transition to orientational order in the film which does not influence the roughness growth modes. For large anisotropies, however, there is a new roughening effect which is accompanied by an increasing amount of particles oriented perpendicularly to the substrate.

The paper is organized as follows: In Sec. II the simulation model is introduced in more detail. In Sec. III results of equilibrium bulk simulations are presented, followed by results of film growth simulations in Sec. IV. Sec. V gives a summary and discusses the relation of this work to experimental results.

II. METHODS

A. Model parameters and observables

The model implemented is an extension of the SOS model presented in Ref. 16, for a schematic picture see Fig. 1. Particles in the lowest layer interact with the substrate with a strength $-\epsilon_{\text{sub}} = E_{\text{particle-substrate}}/(k_{\text{B}}T)$. Additionally, each particle now has a preferred orientation in either the x , y or z direction. If the orientations of two next neighbor (NN) particles are the same as the vector connecting the neighbors, they interact with a strength $-\eta \cdot \epsilon$ (where $\eta \geq 1$ for all of the results below) and $\epsilon = |E_{\text{particle-particle}}|/(k_{\text{B}}T)$. Here, $E_{\text{particle-substrate}}$ and $E_{\text{particle-particle}}$ are interaction energies between a particle and the substrate and between two particles, respectively. If the orientations do not fulfill this condition, they interact with a strength $-\epsilon$. (In Fig. 1, e.g. particle pairs 1-2, 4-5, and 6-7 interact with strength $-\eta\epsilon$ while the other next neighbor pairs interact with $-\epsilon$.) We note that this type of interaction differs from those employed in the well-known Lebwohl-Lasher model²⁶ for the nematic phase in liquid crystals, since in our model alignment of identically oriented particles is only favored along

the axis of orientation (in the Lebwohl-Lasher model, particle pairs 2-3, 4-9, and 7-8 in Fig. 1 would also interact with a strength of $-\eta \cdot \epsilon$, since there equal orientation is favored regardless of the NN position).

The KMC film growth simulations are performed on a cubic lattice of lateral sizes $L = 256$ with periodic boundary conditions in the x and y direction ($z = 0$ defines the substrate plane). In Figs. 6, 7, 12, 13 we show results for $L = 1024$ which confirm the absence of a noticeable finite-size dependence of roughness and order in the film. New particles were inserted into the system at a rate F at a random position on top of the film, respecting the SOS condition (no overhangs). The time Θ is measured via the amount of deposited material, given in units of a filled monolayer. Particles already in the system can either hop to a neighboring site at a rate D (with the restriction that the height difference between the two sites is not more than one lattice site) or change their orientation vector (rotate) at a rate D_{rot} . Both D and D_{rot} are given below in units of the deposition rate F since only the ratios of these kinetic rates matter. D is equivalent to the surface diffusion coefficient for a free particle on the substrate plane or a filled layer. D_{rot} is defined such that for particles with n independent orientations, the concentration c_i of a particle species i relaxes towards the equilibrium value $1/n$ as $c_i(t) = 1/n + (c_i(0) - 1/n) \cdot \exp(-nD_{\text{rot}}t)$ (the time t is in units of $1/F$). In the implementation of rotations we distinguish two cases: Either all particles, including those buried in the bulk of the film, can rotate (henceforth called **Model B**), or only those at the surface (**Model S**). Model B is intuitive for the lattice model as such, since rotations are not sterically blocked. Model S would apply for anisotropically shaped particles which cannot rotate after they have been buried. Hops or rotations are accepted with a probability $p = \min(1, \exp(-\Delta E))$, where ΔE is the change in internal energy this move would cause (in units of $k_{\text{B}}T$). We note that all simulations shown were performed without an Ehrlich-Schwoebel barrier.

A central variable in thin film growth is the roughness of the film, which is defined as

$$\sigma = \sqrt{\frac{1}{N} \sum_{i=1}^N (h_i - \bar{h})^2} \quad (1)$$

where N is the number of lattice sites in the substrate plane, h_i is the height of the film at site i , and \bar{h} is the mean thickness of the film. Furthermore, the average orientation of the film is of interest, described by the order parameter

$$\zeta = \frac{N_z - \frac{1}{2}(N_x + N_y)}{N_x + N_y + N_z} \quad (2)$$

frequently used in the study of liquid crystals. Here, N_α is the number of particles oriented in direction α . ζ varies between -0.5 (all particles are oriented parallel to the substrate plane) and 1 (all particles are oriented along the substrate normal). For an isotropic system it is 0. This observable can be either calculated for the film as a whole or separately for each layer, in which case we denote it as ζ_l .

For the study of the orientational behavior of a bulk film in equilibrium, the following three order parameters are useful:

$$\zeta^{(i)} = \frac{N_i - \frac{1}{2}(N_j + N_k)}{N_i + N_j + N_k} \quad (3)$$

where $i, j, k \in \{x, y, z\}$ and the indices are pairwise different. Note that $\zeta^{(z)} = \zeta$.

B. Relation between interaction and steric anisotropy

With our choice of the interaction anisotropy, we incorporate to some extent an attractive interaction anisotropy for anisotropic molecules. One may assume a van der Waals attraction proportional to the contact area between two molecules. Consider a disc-shaped molecule which is characterized by an orientation vector perpendicular to the disc. The attractive interaction between two such molecules is stronger if the discs are oriented “back-to-back”. In continuum modelling, this is realized e.g. by the Gay-Berne potential for Benzene molecules²⁷. Particle interactions with $\eta > 1$ favor the formation of “fibers” of particles with equal orientation (stacks of discs oriented “back-to-back” if one adopts the perspective from above). Note that such fibers also occur in models of magnetic nano-cubes^{22,28}, in contrast to the interactions there our model has non-polar interactions.

With a slight modification, such a lattice model may also represent rod-like particles. Rods are characterized by an orientation vector along the rod axis, here van der Waals attraction is stronger when the rods are aligned “side-by-side”. In the lattice model, this corresponds to stronger interactions $-\eta\epsilon$ of identically oriented, neighboring particles where the next-neighbor direction is not the orientation direction of the particles. In Fig. 1 the pairs 2-3, 4-9, and 7-8 would have these stronger attractions.

To further mimic steric anisotropies in the disc-like case, we can also define an enhanced substrate interaction of particles oriented perpendicularly to the substrate as $-\eta\epsilon_{\text{sub}}$. This favors lying-down discs as found experimentally for metallic substrates. Such a case will be briefly discussed towards the end of Sec. IV. In the rod-like case, this enhanced substrate interaction energy would apply to x - and y -oriented particles in the first layer.

We see the model setup as a first attempt to represent shape anisotropies solely by interactions. With regard to film growth of anisotropically shaped particles, studies so far have mostly employed molecular dynamics simulations²⁹⁻³¹, which are inherently limited in the system sizes and time scales which can be observed due to their high computational cost. On the other hand, the implementation of a lattice kinetic Monte Carlo (KMC) simulation of these particles poses major challenges regarding the implementations and rates of different moves when particles become elongated³². Simulations of particles with an extension over 2 or 3 lattice sites have been undertaken^{33,34}, concentrating on the (sub-)monolayer regime. Thick films of dipolar

particles extending over 2 lattice sites have been studied in Ref. 35, here understood as growth in a solvent (“colloidal growth”). In these works, a systematic study of film properties on the growth speed and interaction parameters was not undertaken. Off-lattice KMC simulations have also been performed³⁶, but due to the higher number of degrees of freedom, these are again severely limited in the number of particles which can be simulated. Hence the restriction to interaction anisotropy is reasonable.

C. Effective Ehrlich-Schwoebel barrier

In our simulations, there is no explicit Ehrlich-Schwoebel (ES) barrier^{37,38}, $E_{\text{ES}} = 0$. ES barriers can be incorporated asymmetrically (only hops “downwards” have a reduced probability by a factor $\exp(-E_{\text{ES}})$) or symmetrically (hops both upwards and downwards have a reduced probability)³⁹. Interaction anisotropy leads to an effective, asymmetric ES

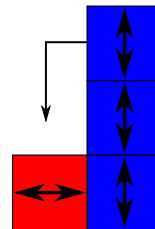


FIG. 2: Schematic illustration for the effective Ehrlich-Schwoebel barrier. For the green particle it becomes energetically unfavorable to hop down when $\eta > 2$.

barrier. Consider a z particle (i.e. a particle oriented in z direction) situated on top of another z particle, as sketched in Fig. 2. The probability $p = \min(1, \exp(-\Delta E))$ for hopping down onto an x or y particle involves the energy change $\Delta E = 2\epsilon - \eta \cdot \epsilon$ and is therefore smaller than 1 for $\eta > 2$, i.e. this hop becomes energetically unfavorable. In turn, the reverse move of hopping up is favored (its probability is 1), one can view this as the effect of an effective asymmetric ES barrier. As shown in Sec. IV D below, for large enough η we find a strong roughening effect which can be traced back to this effective barrier. The exact value of η at which this barrier becomes relevant depends strongly on the kinetic and energetic parameters, since it effectively depends on the average particle environment for downward hops.

D. Remarks on parameter scaling

We investigate ϵ in the range 2..6, $D = 10^3 \dots 10^5$, and $D_{\text{rot}} = 10 \dots 10^4$. A direct comparison to experiments with organic molecules is complicated by the fact that the energetic and kinetic parameters are different from the parameters investigated here, in such experiments typically $\epsilon = 10 \dots 15$ and $D = 10^9 \dots 10^{11}$. However, there are indications that the use of smaller ϵ and smaller D leads to

similar morphological behavior. This holds e.g. for the island density in submonolayer growth in KMC simulations (here the original argument in Ref. 16 is incorrect, but see a correction⁴⁰ based on an analysis of the data of Ref. 11). In the absence of an ES barrier, a scaling relation for the roughness in 3D growth has been found in Ref. 41. Both examples share a dependence on a scaling variable $D^n(c + \exp(-\epsilon))$ where $n \geq 1$ and c is some constant. Therefore, this scaling is only useful for $\epsilon \lesssim -\ln c$ which limits the applicability in monolayer growth to $\epsilon \lesssim 9$ in the monolayer case and $\epsilon \lesssim 4$ in the 3D growth case. For more realistic 3D growth (in the isotropic case), the ES barrier plays an important role. Here, it has been demonstrated in Refs. 42 and 43 that the transition between layer-by-layer and rough 3D growth depends on a scaling variable $D^n \exp(-E_{ES})$. Unfortunately, scaling variables and relations involving all three variables D , ϵ , E_{ES} (for isotropic growth) are not known, and for anisotropic models like the present one the situation is even less clear. In particular, for our choice of D_{rot} there is no experimental justification; the choice of D_{rot} being smaller than D corresponds to assuming (free) energy barriers for rotations to be higher than those for hopping moves.

E. Illustrative snapshots

In Fig. 3, we show three illustrative snapshots from the KMC simulations to representatively highlight the main effects of anisotropy which will be discussed in more detail below. Parameters differ only in the value of the interaction anisotropy parameter η . The other conditions are such that for the isotropic case $\eta = 1$ nearly perfect layer-by-layer (LBL) growth is observed.

In Fig. 3(a), the anisotropy is low ($\eta=1.5$) and the film is isotropic and has grown LBL. With increased anisotropy ($\eta=2.5$ in Fig. 3(b)), one observes a depletion of z -oriented particles (i.e. $\zeta \approx -0.5$) since particles may form energetically advantageous fibers of x -oriented and y -oriented particles (x -fibers and y -fibers, for short) in the film plane by diffusion. The domains composed of x - and y -fibers (red and green in Fig. 3) are small and themselves disordered, hence the fibers are relatively short. The film growth is still LBL. For even higher anisotropy ($\eta=3.5$ in Fig. 3(c)) longer z -fibers (blue in Fig. 3) have formed ($\zeta > 0$) which cause a significantly rougher film and a clear deviation from LBL. The exemplary transitions in Fig. 3 (ordering and roughening) will be examined in more detail below.

III. EQUILIBRIUM BULK PHASE BEHAVIOR

For a thick bulk film, one expects an ordering transition with increasing η . Since the different orientations can be viewed as different particle species, the ordering transition corresponds to a demixing transition between the three species.

In order to determine the location of the equilibrium ordering transition, we performed canonical Monte Carlo

(MC) simulations in a completely filled box of size $L \times L \times L$ with $L = 100$. The system was initialized with randomly oriented particles. A number N_{step} of time steps is performed, during each of which a random particle is selected, a new random orientation was proposed, and then accepted with probability $p = \min(1, \exp(-\Delta E))$, where ΔE is the change in internal energy this rotation would cause. This Metropolis step ensures that, eventually, the system will reach its equilibrium orientation.

For a given ϵ , sweeps of η are performed and for each value of η the three order parameters $\zeta^{(x)}$, $\zeta^{(y)}$, and $\zeta^{(z)}$ are calculated after equilibration. We typically chose 10^{11} steps for equilibration and 10 independent runs for measurement. The value η_{crit} for the ordering transition is found by examining $\zeta_{min,final} = \min_i \zeta^{(i)}$ which exhibits a sharp jump at $\eta = \eta_{crit}$. This is shown in Fig. 4 for the choice $\epsilon = 3$: here one observes the jump at $\eta_{crit} \approx 1.69$ from a disordered system to one in which two particle species dominate and one is depleted ($\zeta_{min,final} < 0$). This is similar to the behavior observed in systems of hard rods on a lattice for intermediate rod lengths^{44,45}. This effect of two dominating species is a consequence of the interactions favoring fibers. Consider planes with $z = \text{const.}$ in their state with lowest energy; these are completely filled with x - or y -fibers (call them x - and y -planes, respectively). There is no energetic difference between two neighboring x -planes or an x -plane next to a y -plane. Entropically, however, it is favorable to allow different orientations in subsequent layers.

From the MC simulations, the transition is found to be well described by

$$\eta_{crit} = 1 + \frac{\chi}{\epsilon} \quad (4)$$

with $\chi \approx 2.07$, as shown in Fig. 5. In Sec. IV below, the η_{crit} found here will be compared to transition values found in growth simulations.

IV. NON-EQUILIBRIUM FILM GROWTH SIMULATIONS

A. Growth modes for isotropic interactions

The first question of interest was whether the interaction anisotropy had any influence on the growth modes observed in Ref. 16, obtained for isotropic particles. Depending on the parameters D , ϵ , and ϵ_{sub} , four growth modes had been identified in Ref. 16: 1) layer-by-layer (LBL), 2) forming islands at first, which then coalesce and form a smooth film (ISL→LBL), 3) forming islands which coalesce into a non-smooth film (ISL→CONST or ISL→3D), and 4) growing a rough film from the beginning (3D). (Here, 3D growth refers to rough, three-dimensional growth and CONST refers to an approximate constant film roughness over time.) Note that for very long times (very thick films), all films roughen and thus show 3D growth⁴¹. There is a rather sharp transition from growth mode 1 to mode 2 upon varying ϵ_{sub} which is reminiscent of a dynamic wetting transition. Also, within

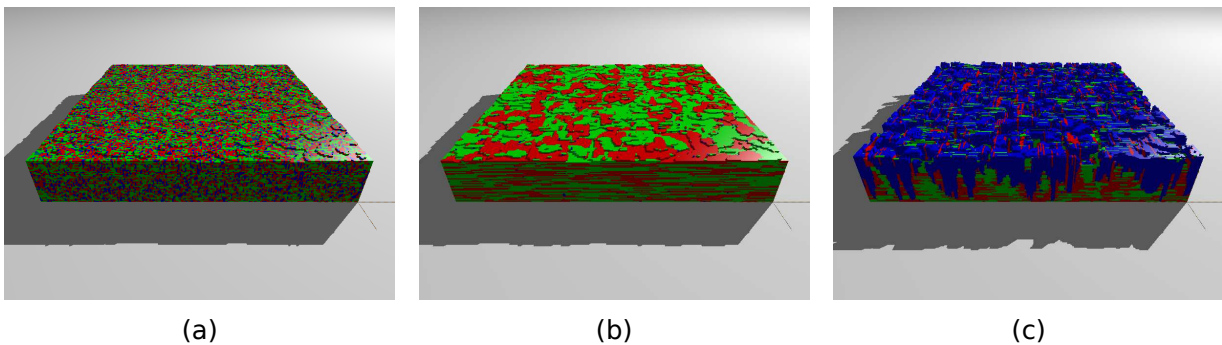


FIG. 3: Snapshots of films after deposition of 50 monolayers at $\epsilon = 3$, $\epsilon_{\text{sub}} = 3.11$, $D = 10^4$, $D_{\text{rot}} = 100$ in model S. The colors red, green, and blue indicate that particles are oriented in the x , y and z direction, respectively. From left to right η increases from 1.5 to 2.5 and 3.5. We see how the film first goes from disordered to ordered without the morphology changing. When increasing η to 3.5, long fibers in the z direction start forming, which lead to a significantly rougher film.

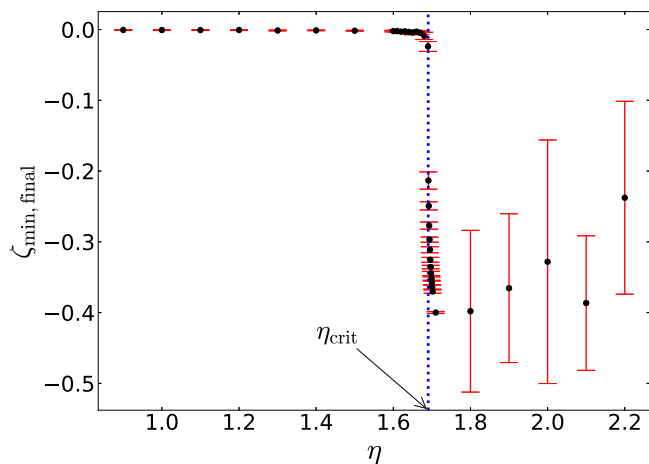


FIG. 4: $\zeta_{\text{min,final}}$ vs η in the canonical equilibrium system for $\epsilon = 3$. For $\eta < \eta_{\text{crit}}$, the system is disordered and all $\zeta^{(i)} \approx 0$. For $\eta \geq \eta_{\text{crit}}$, the system will start phase separating, leading to $\zeta_{\text{min,final}} < 0$

growth mode 2 the change of island growth back to LBL growth happens at a rather sharp time (or coverage Θ) and may be viewed as a “flattening” transition of the film.

B. Growth modes for anisotropic interactions

In Figs. 6 (model S) and 7 (model B) we show typical examples for growth modes 1, 2, and 3 which hold for $\epsilon_{\text{sub}} = 3.11$, 1.78, and 0.89 respectively. The growth mode is read off the roughness curves (upper rows in Figs. 6 and 7). LBL growth ($\epsilon_{\text{sub}} = 0.89$) shows an oscillating small roughness. ISL→LBL growth ($\epsilon_{\text{sub}} = 1.78$) shows an initial sharp growth of roughness which collapses back to an oscillating small roughness. ISL→CONST growth ($\epsilon_{\text{sub}} = 3.11$) shows likewise an initial sharp growth of roughness which collapses back to a nearly constant roughness. Growth mode 4 is not shown here since it only occurs at very high fluxes

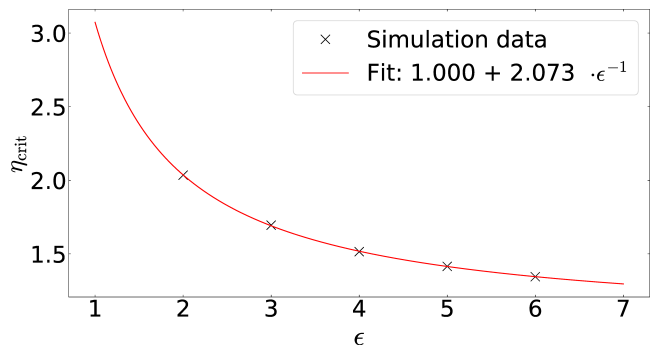


FIG. 5: η_{crit} vs. ϵ in the canonical equilibrium system. The red full line shows a fit of the form $1 + \frac{2.073}{\epsilon}$.

or in the case of a non-vanishing Ehrlich-Schwoebel barrier.

The columns in Figs. 6 and 7 correspond to an increasing anisotropy parameter η between 1 and 2 (from left to right). It is seen that upon increasing η , the system will not change its growth mode, even though the exact roughness values change. There is, however, a significant change in orientational order in the film (see lower rows in Figs. 6 and 7, respectively). For the maximum value $\eta = 2$, the final films in both model S and B are nearly perfectly ordered with $\zeta \approx -0.5$ (all particles are oriented in either the x or y direction). For the intermediate value $\eta = 1.5$ it is seen that for model B the system will initially go towards an ordered state but returns to disorder at higher coverages (Fig. 7). For model S, a partial order remains (Fig. 6).

This indicates that, for sufficiently weak anisotropies, the growth mode and the ordering of the film are independent of each other. Furthermore, for sufficiently thick films, the ordering is also independent of the strength of ϵ_{sub} in both models, due to the short-ranged nature of the substrate attractions. The layer-dependent order parameter ζ_l is constant with increasing l on all substrates for model B, while in model S it shows a gradient.

For weak substrates, $\epsilon_{\text{sub}} = 0.89$, in Figs. 6 and 7, the film grows in mode 3 (ISL→CONST) and the constant rough-

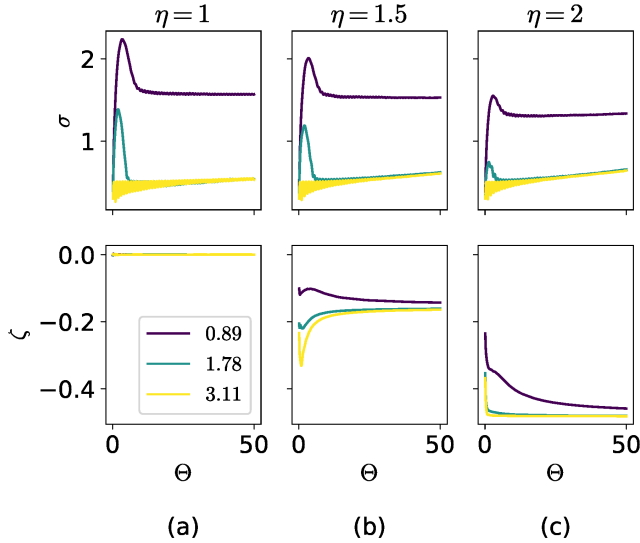


FIG. 6: Roughness σ and order parameter ζ vs Θ for $\epsilon = 3$, $\Gamma = 10^4$, $D_{\text{rot}} = 100$ and $\eta = 1, 1.5, 2$ for different ϵ_{sub} (different colors) in model S (for $L = 1024$). The behavior of σ vs Θ remains the same upon increasing η , while ζ changes from disordered to ordered. Note that $\eta = 1$ corresponds to isotropy, so $\zeta = 0$ is expected.

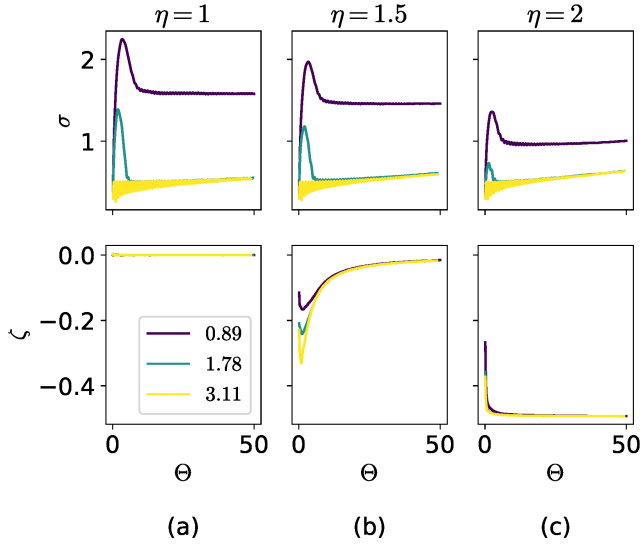


FIG. 7: Same as Fig. 6, but for model B.

ness decreases upon increasing η . One would conjecture that in the limit of very high η , the growth mode of the system will then change to mode 2 (ISL \rightarrow LBL). We observe, however, that above a critical η_{trans} , the film will no longer grow with all particles oriented in parallel to the substrate. Simultaneously, the roughness of the film will increase. This is a non-equilibrium transition (rapid roughening), as shown in Sec. IV D below.

C. Equilibrium transition

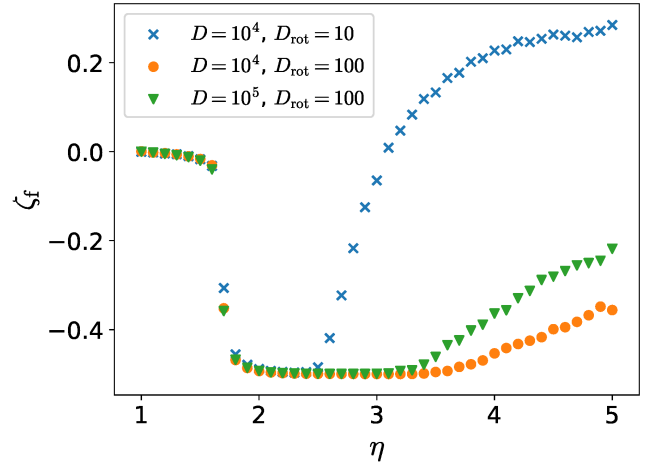


FIG. 8: ζ_f after deposition of 50 ML plotted vs η for $\epsilon = 3$ and $\epsilon_{\text{sub}} = 4$ at different D and D_{rot} in model B. The first transition (from disordered to ordered) is independent of the chosen kinetic parameters.

As shown in the previous section, upon increasing η the system will initially go from an isotropic state to one in which all particles are oriented parallel to the substrate, independent of the strength of ϵ_{sub} . We suspect this to be an equilibrium transition similar to the one found in Sec. III, being independent of the kinetic parameters. For model B, this is shown in Fig. 8, where the final order parameter ζ_f (after deposition of 50 monolayers) vs η is shown for different kinetic parameters. The first transition of ζ_f vs. η is indeed completely independent of the kinetic parameters in the investigated range $D = 10^4 \dots 10^5$ and $D_{\text{rot}} = 10 \dots 100$, indicating equilibrium behavior. After the transition the value of $\zeta_f = -0.5$ indicates that all particles are oriented parallel to the substrate. Note, however, that this is only true in model B. In model S, the system can be frozen in an energetically less favorable state, leading to a ζ_f which is larger than -0.5 .

The critical value η for the disordered \rightarrow ordered transition is extracted from individual $\zeta_f(\eta)$ curves by fitting a tanh function to the data and extracting the inflection point as the transition point η_{crit} (see Fig. 9 for model S and Fig. 10 for model B).

In Fig. 11 the extracted η_{crit} at different values ϵ , re-scaled to $(\eta_{\text{crit}} - 1) \cdot \epsilon$, is shown. In the equilibrium simulations, the re-scaled values are approximately constant, see Eq. (4). For model B, the data are close to this constant value, indicating that the transition is indeed the equilibrium one. In model S, however, this scaling can no longer be found. Here η_{crit} is now significantly lower than the values found for model B. This can be explained by the fact that it is not necessary anymore to re-orient all particles in the film for the transition to occur, but only those at the surface. This leads to the transition occurring at lower

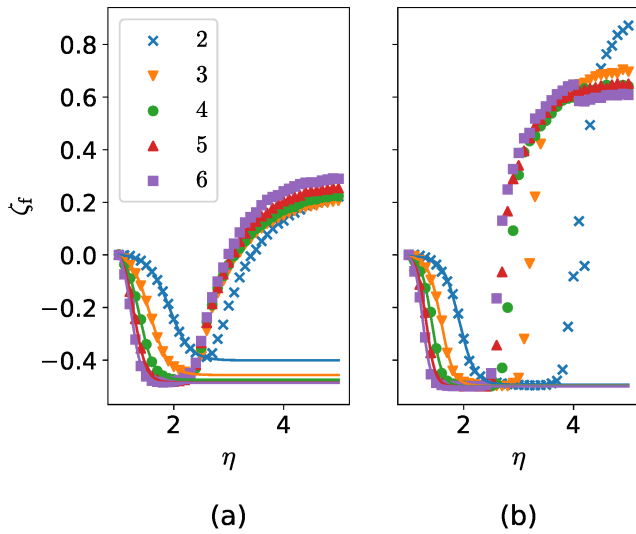


FIG. 9: The order parameter ζ_f after deposition of 50 ML vs η at $\epsilon_{\text{sub}} = 4$, $D = 10^4$ at (a) $D_{\text{rot}} = 10$ and (b) $D_{\text{rot}} = 100$ for different ϵ in model S. The position of the first transition shifts with increasing ϵ . The lines show the fitted tanh, the inflection point of which gives an estimate for the transition point.

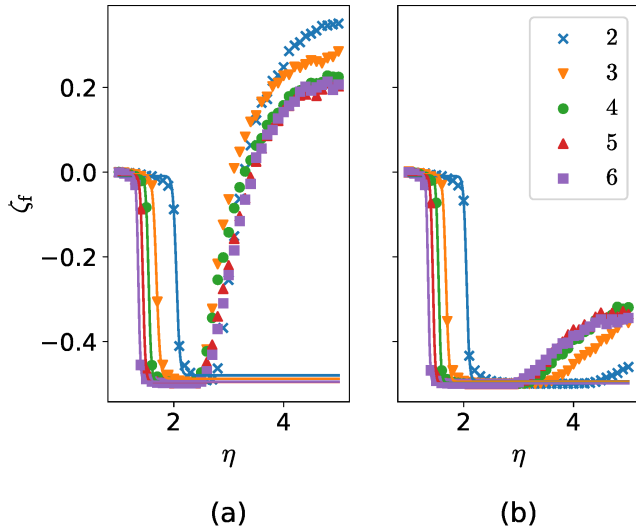


FIG. 10: Same as Fig. 9 but for model B.

anisotropies than in model B.

D. Non-equilibrium transition

In Figs. 8, 9 and 10 it is seen that upon increasing η beyond η_{crit} , the final order parameter ζ_f increases again. The critical η_{trans} for this transition does now depend on the kinetic parameters, indicating that this is a non-equilibrium transition. The increase of ζ is equivalent to the reintroduction of z -oriented particles into the system which for

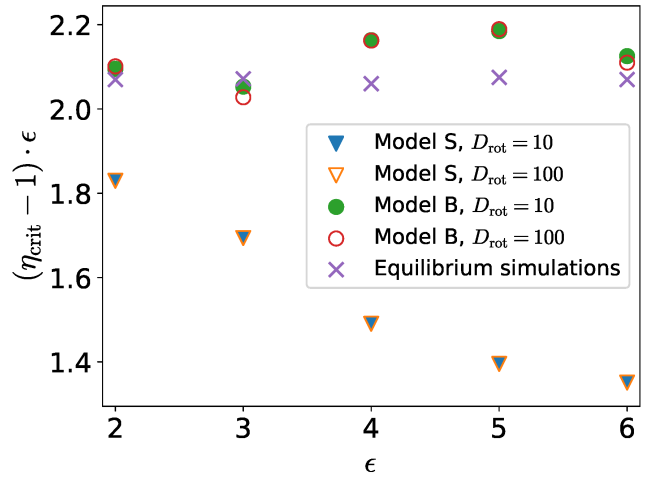


FIG. 11: Critical η for the disordered to ordered transition for different values of ϵ and re-scaled to $(\eta_{\text{crit}} - 1) \cdot \epsilon$.

energetic reasons should be visible in the form of z -fibers in the system. Referring back to Fig. 3(c), the formation of z -fibers is clearly visible.

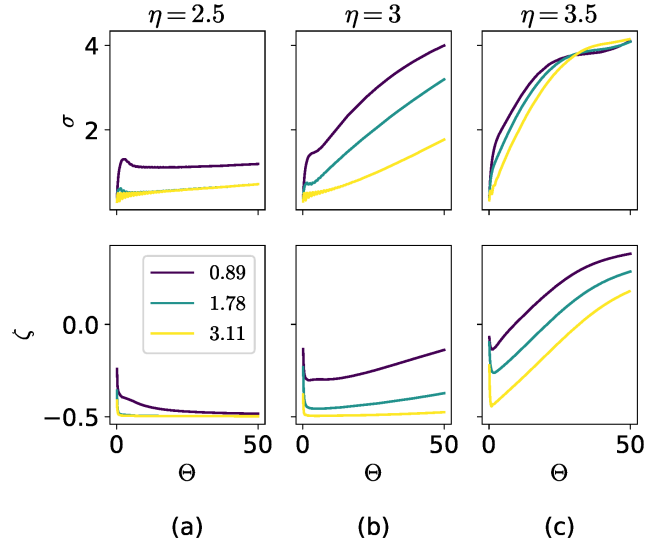


FIG. 12: σ and ζ vs Θ for $\epsilon = 3$, $\Gamma = 10^4$, $D_{\text{rot}} = 100$ and $\eta = 2.5, 3, 3.5$ for different ϵ_{sub} (different colors) in model S (for $L = 1024$). Increasing η past η_{trans} now leads to strong increases in both ζ and σ .

In Figs. 12 (model S) and 13 (model B) the behavior of σ and ζ vs Θ is shown upon further increase of η (these figures are a continuation of Figs. 6 and 7). It is seen that the increase in $\zeta(\Theta)$ after the transition is accompanied with a substantial increase in roughness (rapid roughening). In both models the behavior of $\sigma(\Theta)$ and $\zeta(\Theta)$ strongly deviate from growth under weakly anisotropic conditions, suggesting that they might be used to pinpoint the η_{trans} for non-equilibrium growth. However, as shown in Fig. 14,

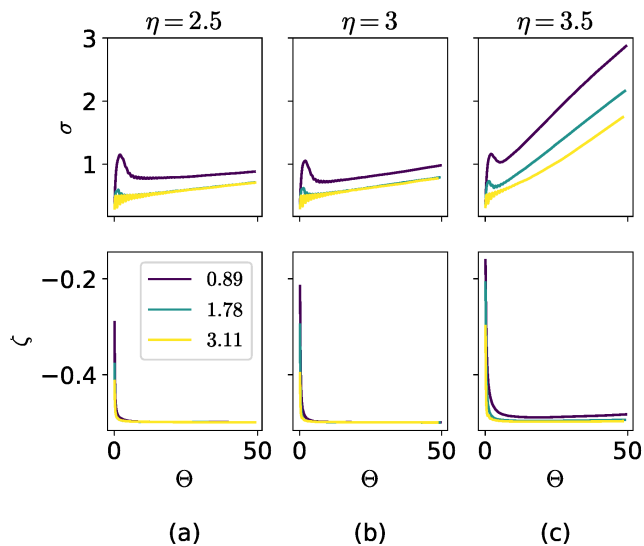


FIG. 13: Same as Fig. 12 but for model B

when plotting e.g. ζ_f vs η , no clear transition point is visible, merely a gradual increase as η is increased. The distributions of fiber lengths do, however, show a clear jump in behavior before and after the transition (see Appendix A). In particular, the distribution of z -fibers shows a significant increase in the average length, in the maximum length and in the width of the distribution. After the transition, fibers can now grow through the whole thickness of the deposited film and reach a maximum length of > 50 lattice sites.

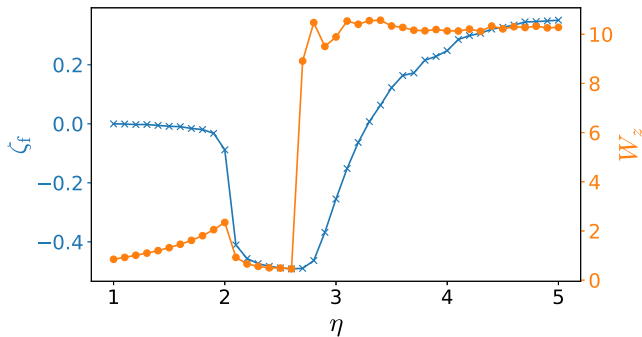


FIG. 14: Comparison of ζ_f and the width W_z of the distribution of z fibers vs η for $\epsilon = 3$, $\epsilon_{\text{sub}} = 4$, $D = 10^4$, $D_{\text{rot}} = 100$ in model S. Both observables show transitions at approximately the same η values. However, σ shows a strong jump at the transition point, due to the onset of the formation of long fibers

Thus, we determined the exact transition point by running 5 simulations for each parameter set (in a system of $L = 100$), measuring the lengths of all z -fibers, and choosing the η at which the width W_z of the z -fiber length distribution (excluding fibers of length 1) jumps to a significantly higher value. This method proved robust enough to determine the critical η for the non-equilibrium transition at a

given ϵ . Notable here was that the transition found through the jump in fiber length occurs slightly before the one we see in ζ_f and that it is much sharper, indicating again that ζ_f is not a good observable to detect such a non-equilibrium transition, since the relative amount of z -fibers is very small initially. Similarly, this also leads to the roughness σ only changing slowly after the transition, making it equally unsuitable for determining the transition point.

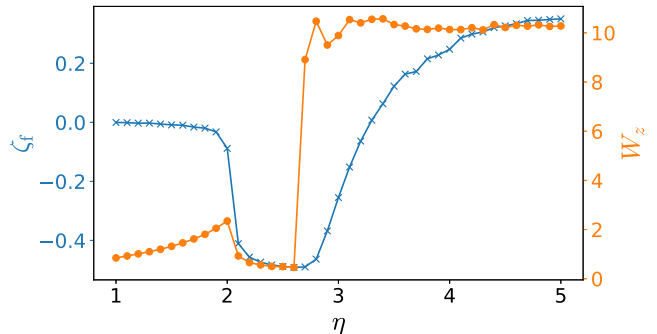


FIG. 15: Heatmap showing the value of η_{trans} for the non-equilibrium roughening transition at different kinetic parameters and $\epsilon = 3$ in model S. Even though the kinetic parameters are varied over several orders of magnitude, η_{trans} only slowly increases at higher D and D_{rot}

We now swept the values of D and D_{rot} over several orders of magnitude and pinpointed the η_{trans} for the non-equilibrium transition for both models B and S. In model B, the non-equilibrium transition could not be observed for η up to 10^5 when both D and D_{rot} are large enough, indicating that such systems will always be in orientational equilibrium if particles can rotate fast enough. In model S, however, there will always be a non-equilibrium roughening transition. Fig. 15 shows a heatmap of η_{trans} as function of D and D_{rot} in model S. We see that, even though D and D_{rot} are varied over several orders of magnitude, η_{trans} will only shift to slightly higher values. In general we can see that an increase in either D or D_{rot} will increase the value of η_{trans} . If D_{rot} is very small, however, the non-equilibrium transition is not very clear. This can be seen especially well for $\log_{10} D_{\text{rot}} \lesssim 2$ in Fig. 15, where increasing D does not necessarily lead to a higher η_{trans} .

Putting together the findings of sections IV C and IV D, one may construct a modified growth mode diagram in the $\epsilon_{\text{sub}} - \eta$ -plane for a given ϵ .

In Fig. 16, this modified growth mode diagram is shown for $\epsilon = 3$. The state of orientational order must be added to the roughness growth modes to describe a combined order-roughness growth mode. For $\eta \lesssim 2.4$ (below the non-equilibrium roughening transition) the roughness modes and film ordering are completely independent of each other. For stronger anisotropies, the system shows a new roughness growth mode (rapid non-equilibrium roughening) which is accompanied by z -fiber formation.

Simulations with the parameters $\epsilon = 4$, $D = 10^4$, $D_{\text{rot}} = 10$ for three substrates $\epsilon_{\text{sub}} = 0.89, 1.78, 3.11$ con-

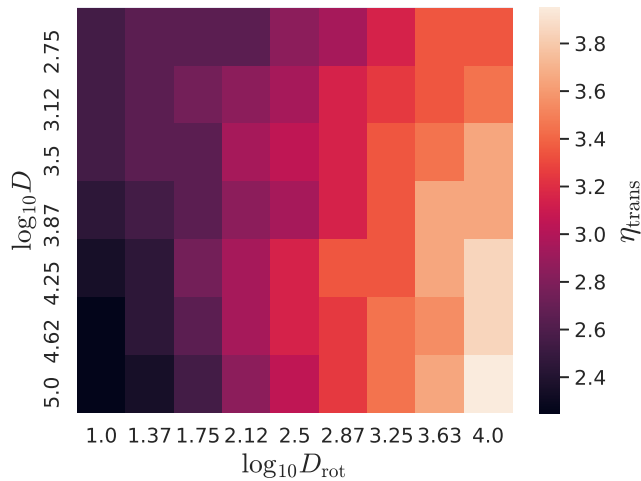


FIG. 16: Modified growth mode diagram for $\epsilon = 3, D = 10^4, D_{\text{rot}} = 10$. Simulated system parameters are shown by symbols, colored regions display approximately the extent of the respective order-roughness growth mode. For $\eta < \eta_{\text{trans}}$, roughness mode and film ordering are independent of each other, leading to 6 kinds of film morphologies in this region. For higher values of η , the film will grow in a non-equilibrium manner, showing sudden changes in both roughness and order parameter

firmed the order and roughness transitions in this phase diagram. The transition values η_{trans} and η_{crit} are shifted to lower values. To cursorily check a possible dependence on D , we performed simulations for $\epsilon = 5, D = 10^5, D_{\text{rot}} = 100$ with $\epsilon_{\text{sub}} = 4$ and varying anisotropy η . As in Fig. 16, the transition *Unordered LBL* \rightarrow *Ordered LBL* \rightarrow *Non-equilibrium roughening* has been found upon increasing η .

E. Strong substrate interactions

So far, all simulations were performed on a substrate which interacts equally strongly with particles of all orientations (“weakly interacting” substrate). We may define “strongly interacting” substrates by setting the substrate interaction of z -oriented particles to $-\eta \epsilon_{\text{sub}}$, which reflects substrates preferring e.g. disk-like particles lying down flat. (In actual growth experiments, metallic substrates are of this kind and for those, surface orientation effects appear to be important; see Sec. V and Ref. 46) As the example for a moderate anisotropy of $\eta = 2$ in Fig. 17 shows, particles in the lowest layer will all be oriented in the z -direction, slowly relaxing to the equilibrium orientations seen in previous systems in higher layers. As a consequence, the total order parameter in the film ζ_f does not reach the equilibrium value of -0.5 (see Fig. 18).

Additionally, it is seen that the non-equilibrium roughening transition is shifted to lower values of η upon switching from the weakly to the strongly interacting substrate. This

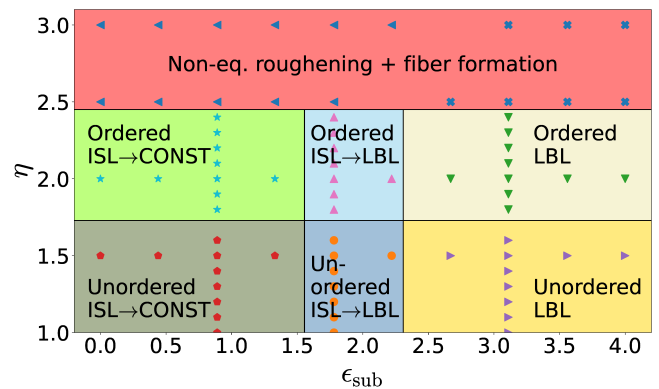


FIG. 17: Layer-dependent order parameter ζ_l vs layer z after deposition of 50 ML in model S for systems in which substrate interaction is (1) ϵ_{sub} for all orientations (weakly interacting substrate) and (2) $\eta \epsilon_{\text{sub}}$ for z -oriented particles (strongly interacting substrate), at $\epsilon = 3$ and $\eta = 2$. We see that on the strongly interacting substrate, the particles are all z -oriented at the substrate, and ζ_l slowly relaxes towards a state of only x - and y -oriented particles in higher layers. On the weakly interacting substrate, there is no change in ordering from lower to higher layers.

can be explained by the fact that the lowest layers are filled with z -oriented particles, acting as nucleation site for growing z -fibers which cause the roughening. Consequently, the new roughening growth mode found for anisotropic particles is further enhanced by strongly interacting substrates.

F. Rod-like interactions

We also investigated systems where the interactions were similar to those of rod-like molecules, i.e. NN particles interact strongly if their orientation is identical, but their positions are not aligned in the direction of the orientation. In Fig. 1, particle pairs 2-3, 4-9, and 7-8 interact with strength $-\eta \epsilon$, while all other particle pairs interact with a strength $-\epsilon$.

In these systems the same behavior was found as for disc-like interactions, only “inverted”. This means that, upon increasing η from 1, the system will first go from a disordered state to one in which all particles are oriented in z -direction (i.e. $\zeta = 1$) (standing-up rods). Upon further increase of η , again a non-equilibrium roughening transition is found, which is accompanied by more particles re-orienting in x and y directions (lying-down rods). For exemplary snapshots and further results for roughness and orientational order in the film, see Appendix B.

We point out that the z -orientation in the film (standing-up rods) here is caused by energetic anisotropy, while for real rod-like molecules one expects strong entropic effects as well. In simulations in which rod-shaped particles (attractive or not) were investigated, it was found that steric repulsions play a crucial role in the ordering behavior, leading e.g. to particles lying down on the substrate and standing

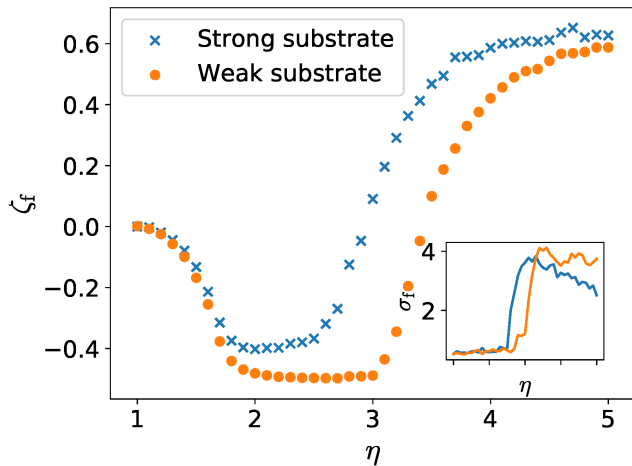


FIG. 18: Comparison of total order parameter ζ in the film after deposition of 50 ML vs. η between strongly and weakly interacting substrates for model S. The disordered \rightarrow ordered transition occurs at the same position in both systems, but non-equilibrium roughening on the strongly interacting substrate is shifted to lower η due to the first adsorbed layer consisting only of z -oriented particles. This earlier transition can also be seen in the behavior of σ_f (see inset). After the transition has occurred in both systems, however, σ_f is lower in the system grown on the strongly interacting substrate.

up upon further filling of the first layer (entropic standing-up transition³²).

V. SUMMARY AND DISCUSSION

We have investigated a lattice SOS model for film growth with anisotropic particles where the anisotropy was modeled via next neighbor attractive interactions which depend upon the orientation of the particles (interaction anisotropy).

The particular choice of interactions was made to (partially) capture the effect of interaction anisotropy for van der Waals-like interacting particles with an anisotropic shape. A new kinetic parameter in such a system is the rotation rate of particles D_{rot} . We distinguished the two cases of model B (all particles in the growing film can rotate) and model S (only surface particles can rotate). If the anisotropy (with associated parameter η) is small, the roughness growth modes identified in an SOS model for isotropic particles¹⁶ are preserved. In this regime we find upon increasing the parameter η (for $\eta < \eta_{\text{trans}}$) that the roughness evolution of the film remains the same as for $\eta = 1$, and the particles in the film become oriented parallel to the substrate. For model B, this orientation transitions is independent of the kinetics of the growing film and takes place at the same value of η as in an equilibrium system. This is somewhat different in model S, but also here the orientation transition is weakly depending on the kinetics and close to the equi-

librium one. This explains the decoupling of roughness and orientation evolution for both rotation models.

For strong anisotropies ($\eta > \eta_{\text{trans}}$), the growth mode is modified. The film will show rapid, non-equilibrium roughening due to the more pronounced occurrence of particles oriented perpendicularly to the substrate forming long fibers, leading to a rougher film and an increased order parameter. In model B, this transition disappears at sufficiently high D and D_{rot} (corresponding to slow growth), since in those cases particles can equilibrate fast enough to reach the (meta-)stable state of parallel orientation adopted in the initial growth. In contrast, in model S, the film will always show this non-equilibrium transition, since buried particles cannot rotate and thus cannot reach their equilibrium orientation.

This strong roughening effect can be rationalized by an inhibition of downhill diffusion for z particles located on top of other z particles, given that the interaction anisotropy is strong enough (higher than $\eta > 2$). In the extreme case with no restrictions on the maximum vertical hop distance, the inhibition of downward hops leads to extremely tall, thin needles of z particles.

The orientation effects we found correspond to the interaction asymmetry of disc-shaped molecules. Actual examples used in organic thin film experimental studies are phthalocyanines (e.g. CuPC and ZnPC), benzene, and perylene. These particles will, given the right conditions, form needles or stacks, similar to particles in our simulations at strong enough anisotropies. The growth direction and ordering of such needles also strongly depends on the substrate. Notable here are amorphous substrates, such as SiO_2 (corresponding to a weakly interacting substrate in our work) and ordered substrates, such as metal surfaces (corresponding to a strongly interacting substrate).

Experiments with phthalocyanines on an amorphous substrate have shown that the disc-like molecules stand upright on the substrate and form needles consisting of herringbone like arranged particles growing in all directions parallel to the substrate⁴⁷. On metallic substrates, particles in the first layer will lie flat on the substrate, initiating needle-growth perpendicular to the substrate, see⁴⁸ for perylene growth on copper or^{49,50} for HBC on Cu(111) and Au(111). These results are reminiscent of behaviors we found in simulations using weakly and strongly interacting substrates, respectively. For benzene and benzene derivatives it has been observed that, depending on the substrate material, benzene thin films will either form needles which are stable throughout the whole growth process⁵¹ or they will form ordered structures in the first layer, but random crystallites in higher layers⁵¹ (similarly for the derivative 1,3-bis(N-carbazolyl)benzene (mCP)⁵²). Such behavior we find here for particles with a relatively low anisotropy ($1 < \eta < \eta_{\text{crit}}$) growing on strongly and weakly interacting substrates, respectively. In Ref. 53 it was found that when increasing the substrate temperature when depositing benzene onto gold-coated copper, the film ordering will go from amorphous (glassy) to partially crystallized to completely crystallized. This does not match well our findings that, for a given η ,

decreasing ϵ (increasing T) will move the film from a non-equilibrium roughened phase to an equilibrium phase (there is no glassy phase in our model). However, here the correspondence is not as clear since changing T will also change D and D_{rot} .

An open question is whether needle-formation as described also leads to the kind of strong roughening we found in our simulations. Quantitative determinations of roughness evolution with time for disc-like molecules is scarce. An example for CuPC growth on SiO₂ seems to agree with this trend⁵⁴. However, for a confirmation of orientation-dependent strong roughening one would need information on both roughness and the orientation in the film, otherwise strong roughening can be easily due to strong Ehrlich-Schwobell barriers. A second example is the study in Ref. 55 for F₁₆CuPc on SiO₂ which shows a strong roughening after approx. 40 nm of film thickness (~ 27 layers of standing-up discs) which is clearly accompanied by a change in the type of surface grains but the orientation of the molecules after the strong roughening is unclear.

A wealth of data and observations can be found for thin film growth with rod-like molecules, most notably pentacene (PEN) and diindenoperylene (DIP). Here a strong roughening effect is found which is not seen in our model. For PEN and DIP growth on a weakly interacting substrate (SiO₂ at high enough temperature) there is initial LBL growth of standing-up rods for a few layers which changes into fairly strong 3D growth⁵⁶⁻⁶⁰ and it does not seem to be accompanied by an appearance of lying-down rods. On the other hand, the appearance of islands of lying-down rods and ensuing roughening (as in our model, see App. B) is seen for DIP on SiO₂ at lower temperatures⁵⁶ and for DIP on gold⁴⁶. PEN does not show such an effect for SiO₂ at lower temperatures but a 1:1 mixture of PEN:PFP (perfluoropentacene) does⁶¹. PEN on gold exhibits a lying-down monolayer and subsequent layers with predominantly standing-up

molecules⁶², similar to the order behavior shown in Fig. 18 but roughness data are not available.

We have mainly discussed the relation to experimental results for growth of molecules in a vacuum chamber. The experimental conditions for growth in a colloidal system are quite different, as manifest in bulk diffusion of material above the film and the range and magnitude of interparticle interactions⁶³. Nevertheless, direct measurements of island growth reveal also many similarities⁶⁴, and in our previous KMC simulation the differences between a colloidal growth model (with bulk diffusion) and an SOS model were found to be small¹⁶. Therefore, our results should also be applicable to colloidal growth, in this respect dedicated experiments with film growth of anisotropic particles are desirable.

Summarizing, the simplified anisotropic model of this work captures some trends seen in experimental work with disc-like molecules as well as for rod-like molecules. Strong roughening for rod-like molecules without an apparent strong change in molecular orientation point to the necessity of including steric interactions. Nevertheless, we think that it is useful to identify general effects of anisotropy and resulting trends on the ordering and roughness behavior of thin films using simplified, generic models. An obvious extension of the model used in this work would be to include simple anisotropic shapes of the lattice particles, which requires more detailed considerations on the admissible moves and kinetic parameters in the system and would be computationally more expensive.

ACKNOWLEDGMENTS

We thank Frank Schreiber for various insightful discussions and his helpful suggestions in finalizing this manuscript. We gratefully acknowledge financial support of the German Research Foundation (Deutsche Forschungsgemeinschaft, DFG) through project Oe 285/3-1.

-
- [1] W. Brütting and C. Adachi, *Physics of organic semiconductors* (Wiley-VCH, 2012), 2nd ed.
 - [2] J. Yang and D. Yan, *Chem. Soc. Rev.* **38**, 2634 (2009).
 - [3] J. Evans, P. Thiel, and M. Bartelt, *Surf. Sci. Rep.* **61**, 1 (2006).
 - [4] S. Clarke and D. D. Vvedensky, *J. Appl. Phys.* **63**, 2272 (1988).
 - [5] O. Venäläinen, J. Heiniö, and K. Kaski, *Phys. Scripta* **T38**, 66 (1991).
 - [6] K. Binder, *Rep. Prog. Phys.* **60**, 487 (1997).
 - [7] D. Blömker, C. Gugg, and M. Raible, *Eur. J. Appl. Math.* **13**, 385 (2002).
 - [8] E. E. M. Luis, I. S. S. Carrasco, T. A. de Assis, and F. D. A. Aarão Reis, *Phys. Rev. E* **102**, 012805 (2020).
 - [9] T. B. To, R. Almeida, S. O. Ferreira, and F. D. A. Aarão Reis, *Appl. Surf. Sci.* **560**, 149946 (2021).
 - [10] T. Martyneć and S. H. Klapp, *Phys. Rev. E* **100**, 033307 (2019).
 - [11] T. Martyneć, C. Karapanagiotis, S. H. L. Klapp, and S. Kowarik, *Commun. Mater.* **2**, 90 (2021).
 - [12] O. Pierre-Louis, A. Chame, and Y. Saito, *Phys. Rev. Lett.* **99**, 136101 (2007).
 - [13] O. Pierre-Louis, A. Chame, and M. Dufay, *Eur. Phys. J. B* **77**, 57 (2010).
 - [14] A. Pimpinelli and J. Villain, *Physics of Crystal Growth* (Cambridge University Press, 1998).
 - [15] T. Michely and J. Krug, *Islands, mounds, and atoms: patterns and processes in crystal growth far from equilibrium* (Springer, 2004).
 - [16] E. Empting, M. Klopotek, A. Hinderhofer, F. Schreiber, and M. Oettel, *Phys. Rev. E* **103**, 023302 (2021).
 - [17] T. B. To and F. D. A. Aarão Reis, *J. Alloys Compd.* **835**, 155093 (2020).
 - [18] L. Mederos, E. Velasco, and Y. Martínez-Ratón, *J. Phys.: Condens. Matter* **26**, 463101 (2014).
 - [19] P. Quiring, M. Klopotek, and M. Oettel, *Phys. Rev. E* **100**, 012707 (2019).
 - [20] P. A. Lebowitz and G. Lasher, *Phys. Rev. A* **6**, 426 (1972).

- [21] G. Luckhurst and S. Romano, *Mol. Phys.* **40**, 129 (1980).
- [22] X. Zhang, Z. Zhang, and S. C. Glotzer, *J. Phys. Chem. C* **111**, 4132 (2007).
- [23] T. Martynec and S. H. L. Klapp, *Phys. Rev. E* **98**, 042801 (2018).
- [24] S. Bommel, N. Kleppmann, C. Weber, H. Spranger, P. Schäfer, J. Novak, S. V. Roth, F. Schreiber, S. H. L. Klapp, and S. Kowarik, *Nat. Comm.* **5**, 5388 (2014).
- [25] W. Janke and T. Speck, *J. Chem. Phys.* **154**, 234701 (2021).
- [26] M. A. Bates, *Phys. Rev. E* **64**, 051702 (2001).
- [27] P. A. Golubkov and P. Ren, *J. Chem. Phys.* **125**, 064103 (2006).
- [28] M. W. Szyndler and R. M. Corn, *J. Phys. Chem. Lett.* **3**, 2320 (2012).
- [29] L. Muccioli, G. D'Avino, and C. Zannoni, *Adv. Mater.* **23**, 4532 (2011).
- [30] O. M. Roscioni, G. D'Avino, L. Muccioli, and C. Zannoni, *J. Phys. Chem. Lett.* **9**, 6900 (2018).
- [31] S. Ikeda, *Appl. Phys. Express* **13**, 015508 (2020).
- [32] M. Klopotek, H. Hansen-Goos, M. Dixit, T. Schilling, F. Schreiber, and M. Oettel, *J. Chem. Phys.* **146**, 084903 (2017).
- [33] D. Choudhary, P. Clancy, R. Shetty, and F. Escobedo, *Adv. Funct. Mater.* **16**, 1768 (2006).
- [34] M. Haran, J. E. Goose, N. P. Clote, and P. Clancy, *Langmuir* **23**, 4897 (2007).
- [35] J. Huang and G. Liu, *J. Phys. Chem. C* **115**, 5385 (2011).
- [36] T. Neumann, D. Danilov, C. Lennartz, and W. Wenzel, *J. Comput. Chem.* **34**, 2716 (2013).
- [37] G. Ehrlich and F. G. Hudda, *J. Chem. Phys.* **44**, 1039 (1966).
- [38] R. L. Schwoebel, *J. Appl. Phys.* **40**, 614 (1969).
- [39] F. F. Leal, T. J. Oliveira, and S. C. Ferreira, *J. Stat. Mech. Theory Exp.* **2011**, P09018 (2011).
- [40] E. Empting, M. Klopotek, A. Hinderhofer, F. Schreiber, and M. Oettel, *Phys. Rev. E* (submitted) (2022).
- [41] T. A. de Assis and F. D. A. Aarão Reis, *J. Stat. Mech.: Theory Exp.* **2015**, P06023 (2015).
- [42] V. I. Trofimov and V. G. Mokerov, *Comput. Mater. Sci.* **17** (2000).
- [43] V. I. Trofimov, I. V. Trofimov, and J. I. Kim, *Comput. Mater. Sci.* **33**, 362 (2005).
- [44] A. Gschwind, M. Klopotek, Y. Ai, and M. Oettel, *Phys. Rev. E* **96**, 012104 (2017).
- [45] N. Vigneshwar, D. Dhar, and R. Rajesh, *J. Stat. Mech.: Theory Exp.* **2017**, 113304 (2017).
- [46] A. C. Dürr, N. Koch, M. Kelsch, A. Rühm, J. Ghijsen, R. L. Johnson, J.-J. Pireaux, J. Schwartz, F. Schreiber, H. Dosch, et al., *Phys. Rev. B* **68**, 115428 (2003).
- [47] Z. Bao, A. J. Lovinger, and A. Dodabalapur, *Adv. Mater.* **9**, 42 (1997).
- [48] K. Hänel, S. Söhnchen, S. Lukas, G. Beernink, A. Birkner, T. Strunskus, G. Witte, and C. Wöll, *J. Mater. Res.* **19**, 2049 (2004).
- [49] P. Beyer, T. Breuer, S. Ndiaye, A. Zykov, A. Viertel, M. Gensler, J. P. Rabe, S. Hecht, G. Witte, and S. Kowarik, *ACS Appl. Mater. Interfaces* **6**, 21484 (2014).
- [50] P. Ruffieux, O. Gröning, M. Biemann, C. Simpson, K. Müllen, L. Schlapbach, and P. Gröning, *Phys. Rev. B* **66**, 073409 (2002).
- [51] H. Yuan, K. Gibson, D. R. Killelea, and S. Sibener, *Surf. Sci.* **609**, 177 (2013).
- [52] S. Kwon, T. G. Kim, W. K. Choi, S. O. Kang, and J. W. Kim, *ACS Appl. Mater. Inter.* **5**, 1896 (2013).
- [53] K. Ishii, H. Nakayama, T. Yoshida, H. Usui, and K. Koyama, *B. Chem. Soc. Jpn.* **69**, 2831 (1996).
- [54] B. Reisz, E. Empting, M. Zwadlo, M. Hodas, G. Duva, V. Belova, C. Zeiser, J. Hagenlocher, S. Maiti, A. Hinderhofer, et al., *Phys. Rev. Mater.* **5**, 045601 (2021).
- [55] J. Yang, S. Yim, and T. S. Jones, *Sci. Rep.* **5**, 9441 (2015).
- [56] A. Dürr, B. Nickel, V. Sharma, U. Täffner, and H. Dosch, *Thin Solid Films* **503**, 127 (2006).
- [57] X. Zhang, E. Barrena, D. de Oteyza, and H. Dosch, *Surf. Sci.* **601**, 2420 (2007).
- [58] S. Kowarik, A. Gerlach, W. Leitenberger, J. Hu, G. Witte, C. Wöll, U. Pietsch, and F. Schreiber, *Thin Solid Films* **515**, 5606 (2007).
- [59] S. Kowarik, A. Gerlach, M. W. A. Skoda, S. Sellner, and F. Schreiber, *Eur. Phys. J. Spec. Top.* **167**, 11 (2009).
- [60] H. Zhu, Q. L. Li, X. J. She, and S. D. Wang, *Appl. Phys. Lett.* **98**, 243304 (2011).
- [61] A. Hinderhofer, C. Frank, T. Hosokai, A. Resta, A. Gerlach, and F. Schreiber, *J. Chem. Phys.* **134**, 104702 (2011).
- [62] D. Käfer, L. Ruppel, and G. Witte, *Phys. Rev. B* **75**, 085309 (2007).
- [63] N. Kleppmann, F. Schreiber, and S. H. L. Klapp, *Phys. Rev. E* **95**, 020801(R) (2017).
- [64] R. Ganapathy, M. R. Buckley, S. J. Gerbode, and I. Cohen, *Science* **327**, 445 (2010).

Appendix A: Distributions of fiber lengths

In Sec. IV D, the transition points for the strong roughening transition for higher anisotropies were determined using the width of the distribution of z fibers which exhibits a significant jump at the transition value η_{trans} of the non-equilibrium transition. In Fig. 19 an explicit example for the length distribution of x -, y - and z -fibers just before and just after the transition is shown which illustrates the origin of this behavior. In Fig. 19(a) at $\eta < \eta_{\text{trans}}$, the length distribution of z -fibers is narrow, not exceeding a length of 7 while lengths of x - and y -fibers may reach the box length and in Fig. 19(b) at $\eta > \eta_{\text{trans}}$, the length distribution of z -fibers is significantly wider, with fiber lengths going up to almost 50 (the final average film thickness). The distribution only weakly depends on the length which is also the cause for a large width of the distribution. This behavior of the z -fiber length distribution was found for all parameters investigated in Fig. 15.

Appendix B: Rod-like interactions

As discussed in Sec. IV F, the case of interaction anisotropy emulating rod-like shapes leads to a qualitatively similar behavior as in the disc-like case. We illustrate this first with snapshots of the final film morphology for increasing anisotropy parameter, see Fig. 20. (These snapshots should be compared with those in Fig. 3 for the disc-like case.) Fig. 3(a) shows a film of isotropic particles ($\eta = 1$), grown in LBL. There is a random distributions of

particle orientations in the film. Fig. 3(b) is for moderate anisotropy ($\eta = 1.6$) the film is almost completely ordered with standing-up rods (first, equilibrium transition) but LBL growth has not changed. Fig. 3(c) is for strong anisotropy ($\eta = 3.0$), and x -, y -oriented particles (lying-down rods) have appeared which are energetically favored growing in perpendicular, wall-like segments. Thermal motion and the finite deposition speed lead to domains of x -, y -oriented particles whose size is larger and whose lateral shape is more compact than found for the z -fibers in the disc-like case (see Fig. 3(c) for a comparison). The domains lead to an increased roughness of the film (rapid roughening transition).

In Fig. 21 we show the order parameter ζ_f and the roughness σ_f vs η for different values of ϵ . The transitions in ζ_f are now opposite to those observed for disc-like interaction, i.e. the first transition is from an unordered phase to one in which all particles are oriented in the z direction (ζ goes from 0 to 1), while at even higher values of η the order parameter will decrease again in what appears to be a non-equilibrium transition. This is an inversion of the behavior seen for disc-like particles, but qualitatively the transitions are identical. For $\eta > \eta_{\text{trans}}$, there seems to be no significant dependence of σ_f on ϵ . σ_f reaches approximately the same values as in the disc-like system, due to x and y particles now forming wall segments, not fibers, with identically oriented particles, strongly roughening the surface (Snapshots shown in Fig. 20).

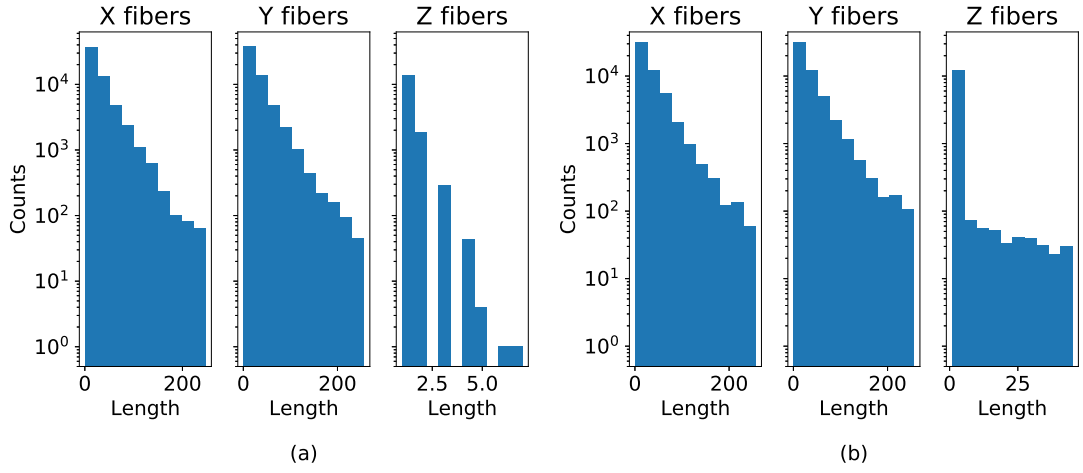


FIG. 19: Fiber length distributions (a) before and (b) after the non-equilibrium transition at $\epsilon = 2$, $D = 10^4$, $D_{\text{rot}} = 10$ and (a) $\eta = 2.6$, (b) $\eta = 2.7$

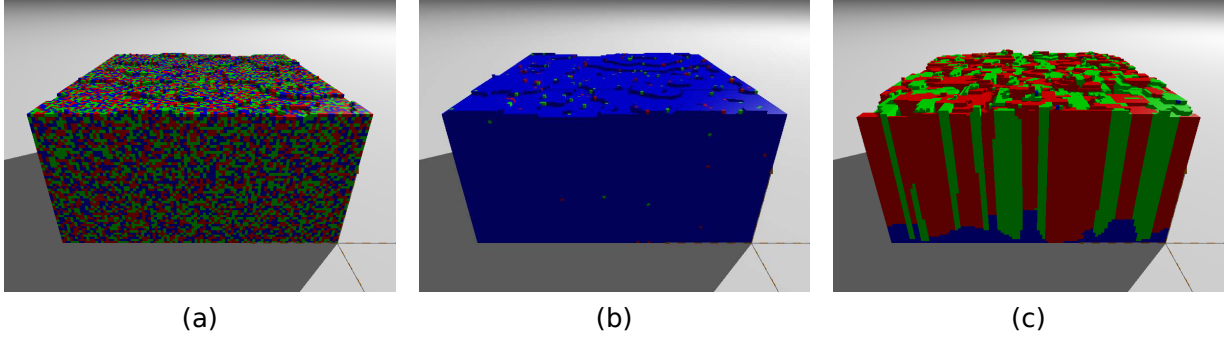


FIG. 20: Snapshots of films after deposition of 50 monolayers at $\epsilon = 3$, $\epsilon_{\text{sub}} = 3.11$, $D = 10^4$, $D_{\text{rot}} = 100$ in model S for rod-like interactions. The colors red, green, and blue indicate that particles are oriented in the x , y and z direction, respectively. From left to right η increases from 1 to 1.6 and 3. We see how the film first goes from disordered to ordered without the morphology changing. When increasing η to 3, x and y particles start forming planes, roughening the film

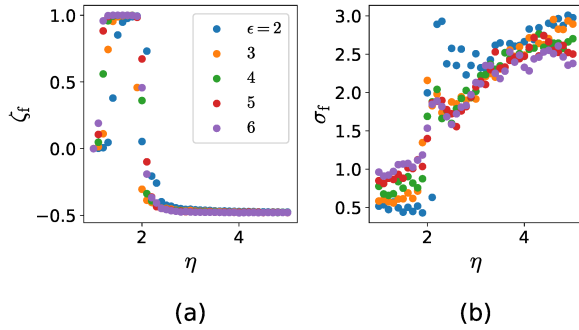


FIG. 21: (a) ζ_f and (b) σ_f after deposition of 50 ML vs η at $\epsilon_{\text{sub}} = 4$, $D = 10^4$ and $D_{\text{rot}} = 100$ for different ϵ in model S.